 https://doi.org/10.3011/ESARDA.IJNSNP.2020.10

Three-dimensional Positional Analysis of Weapons Grade Plutonium Using Gridded Arrays of Dosimeters

Ryan P O'Mara[1] and Robert B Hayes[2]

[1] Pacific Northwest National Lab
902 Battelle Boulevard, Richland WA 99354
[2]North Carolina State University
Nuclear Engineering Department
2500 Stinson Dr. Raleigh, NC 27520
E-mail: ryan.omara@pnnl.gov

Abstract:

One of the primary challenges to preventing the covert proliferation of nuclear weapons is that no technology currently exists that can economically monitor nuclear activities continuously throughout time. Previous studies have shown that luminescence dosimetry can potentially be used to determine the energy of historical radiation environments and even source positions. This work serves to demonstrate that with an adequate number of radiation dose measurements, it may also be possible to image source material using luminescence dosimetry. To that end, a 4.5 kg sphere of weapons grade plutonium was used to expose two gridded arrays of commercial optically stimulated luminescence dosimeters (OSLDs). The measured position-wise dose was then used to reconstruct the 3-dimensional position of that source material. Expanding upon these findings it may be possible in the future to use luminescence dosimetry in ubiquitous, environmental materials to reconstruct the historical radiation fields in nearly any nuclear facility in the world. Developing such a capability could greatly increase the likelihood of detection of covert nuclear weapons development across broad time scales.

Keywords: Nonproliferation, verification technologies, radiation detection, passive detection

1. Introduction

Luminescence dosimetry has long been a mainstay in the realms of personnel and accident dosimetry, however recent advances have demonstrated these new techniques may also have a place in nuclear nonproliferation and treaty verification. Previous research has shown that using a combination of optically stimulated luminescence (OSL) and thermoluminescence (TL) allows for the assay of nuclear material with surprising resolution [1]. Likewise, doses to surface mount resistors (SMRs), like those found in common personal electronics, have been measured down to background levels using OSL [2]. Even more recently, a linear array of commercially available optically stimulated luminescence dosimeters (OSLDs) were used to localize the position of a weapons grade plutonium (WGPu) source [3]

One of the principle challenges with respect to weapons treaty verification is that many conventional measurement techniques can reveal classified or protected information about the weapons. As a result, signatories of such treaties would be expected object to the use of such instrumentation for verification activities. Gross dose rate information, such as that measured by luminescence dosimeters, on the other hand, can be expected to be much more palatable to treaty signatories since it is unlikely to contain protected design information.

The purpose of this work is to build upon prior studies to show the plethora of information that can be acquired using dose deposition in ubiquitous materials. While the present study was performed using commercial OSLDs, the same data could potentially be obtained from any number of materials ranging from structural bricks to crystalline particulate matter in dust.

1.1 Analytical Source Position Analysis

As done previously [3] when using a single linear distribution of OSLDs, the positions of a spherical source can be approximated as a point source. Under this approximation, the linear array of measured doses will follow the functional form of

$$Y = m_1 / \left(m_2^{\,2} + \left(Z - m_3 \right)^2 \right), \tag{1}$$

where m_2 is the radial position estimate and m_3 axial position estimate, in cylindrical coordinates. In Equation (1), the m_1 parameter is then simply related to the magnitude of the dose delivered. Under this coordinate system, the "z-axis" is the line connecting the linear array of dosimeters. Applying Equation (1) for a single linear array of detectors, it was shown that the position of the source could be determined with a 1° angular resolution [3].

Hayes and O'Mara [3] also showed that by coupling forward particle transport solutions with black-box optimizations routines, the source position and radius could also be simultaneously determined. It was noted, however, that using the full transport solutions were computationally expensive. As a result, it would be advantageous to use simplified methods, such as applying Equation (1), to solve for the approximate source position and then use the more

 O'Mara, R.P., & Hayes, R.B. (2020). Three-dimensional Positional Analysis of Weapons Grade Plutonium Using Gridded Arrays of Dosimeters. *ESARDA Bulletin - The International Journal of Nuclear Safeguards and Non-proliferation*, 61, 32-38. https://doi.org/10.3011/ESARDA.IJNSNP.2020.10

computationally expensive routines only to solve for other source characteristics, such as the radius. This work builds upon the results reported by Hayes and O'Mara [3], by illustrating a method by which a gridded array (or simply orthogonal linear arrays) can be used to solve for the three-dimensional position of a source. The resultant position could then be used in subsequent full transport models to determine other source characteristics.

2. Materials and Methods

All measurements were made in June of 2019 at the Device Assembly Facility (DAF) at the former Nevada Test Site. The source under investigation was a 4.48-kg sphere of WGPu with a diameter of 7.5876 cm. The WGPu sphere was constructed in 1980 with initial isotopic weight percentages of .02, 93.735, 5.95, 0.2685 and 0.028 for the isotopes of ^{238}Pu, ^{239}Pu, ^{240}Pu, ^{241}Pu and ^{242}Pu respectively with 557 ppm of ^{241}Am.

Two arrays composed of nanodot OSLDs, by Landauer, taped to a foam board backing were constructed and exposed to the source for 85.7 hours. The first OSLD array, termed the large array (LA), was built on a foam board that measured 135 cm long by 90 cm wide. The LA consisted of a 10-by-10 array of OSLDS where the OSLDs on the long axis had a center-to-center spacing of 15 cm and those on the short axis had a center-to-center spacing of 10 cm. The second array, the small array (SA), consisted of an 8-by-8 array of OSLDs, with center-to-center spacings of 10 cm and 7 cm on the long and short axes, respectively. The foam board backing for the SA measured 70 cm by 49 cm in total.

Figure 1 shows the outer configuration of the OSLD arrays with the source in place. It can be seen from the image that the LA was suspended parallel to the floor, above the source using two utility carts. The SA was secured perpendicular to the LA on one of the utility carts. It can also be seen that the source was placed offset from the center of the LA, 20 cm closer to the utility cart supporting the SA.

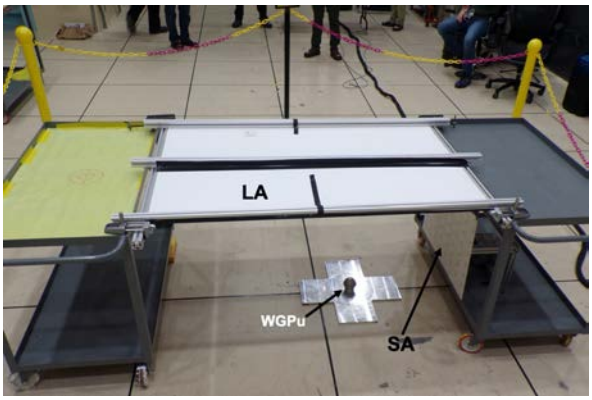

Figure 1: Outer view of the dosimeter arrays. The LA has dosimeters on the opposite side seen here with the SA having dosimeters visible. The clad WGPu was placed on a cross plate of Al on the floor composed of tile on top of concrete.

Figure 2 shows the position of the source from floor level. It can be seen here that the entirety of the SA is positioned above the source. As such, there is no line of OSLDs bisecting the source perpendicular to its central axis where the cladding has a lip. Also shown in Figure 2 is the aluminium stand that the source rests on. The benefit of having both arrays above the source was to reduce the shadowing effect by this stand and to reduce the albedo effect from the floor primarily from the metal cross upon which the WGPu was positioned (Figure 1). There is also a cladding lip around the WGPu which is partially shadowing the lower half of the WGPu to the SA but not the LA as shown in Figure 2.

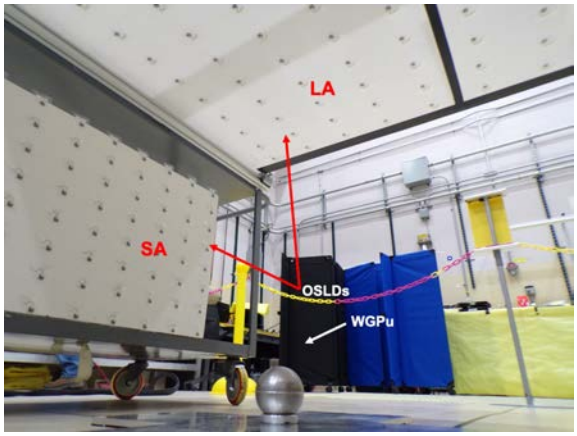

Figure 2: Underside of the exposure geometry, showing the weapons grade plutonium source and both of the dosimeter arrays.

2.1 OSLD Measurement

The dose to each of the OSLDs was measured using a Landauer microStarii® medical dosimetry unit. Prior to the measurement of the OSLD doses, a set of known exposure (NIST traceable doses) OSLDs were utilized to ensure the constancy of the unit calibration and dose estimates. Each dosimeter was read a single time; however, each read consists of a dose estimate from four individual LED pulses. The resultant dose estimate is then the average of the four pulses and the dose uncertainty is its standard deviation.

The nanoDOT™ OSLDs are all calibrated for exposures perpendicular to the top surface of the dosimeter cassette and as a result the dose etimates from the nanodots can be somewhat sensitive to the angle of the dosimeter relative to the irradiation source [4]. The angular dependence of the dosimeters was calculated by a Monte Carlo simulation using MCNP6® [5]. The source's photon spectrum was determined using the Origen module of the SCALE package [6]. The Origen calculation was used to decay the original, measured source material by 39 years and determine the expected present-day isotopic compositions and gamma source rate term. Only those gamma source rate terms with relative contributions greater than 1E-8 were included in the final source specification for the particle transport simulations. The source term was uniformly spread throughout the volume of

the modeled plutonium sphere, in order to account for self-shielding effects.

The photon dose deposition in the Al_2O_3:C chip within each dosimeter set was calculated using a pulse height, energy deposition (*F8) tally. The *F8 tally provides the energy distribution of "pulses" created in a cell modeled as a physical detector [5]. The source spectrum from the Origen calculation was transported mono-directionally at various angles relative to the surface of the simulated dosimeter. Finally, the angular correction factor was calculated as the ratio of the calculated dose deposition for an angle θ to the calculated dose deposition at 90°. The dose measurement for each dosimeter was multiplied by the correction factor calculated for the angle between the dosimeter and the center of the source.

2.2 Source Position Analysis

For each of the two dosimeter arrays, Equation (1) was first fit (using the Levenberg-Marquardt (LM) method) to measured dose profiles both row and column-wise, in order to obtain estimates for each of the two coordinates in the plane of the array (see Figure 3). The final coordinate estimates were calculated as the variance-weighted average of all of the m_2 parameters from the fit to each dosimeter row (or column). Next, the estimated in-plane coordinates were used to calculate the perpendicular distance between the source and the dosimeter plane using the m_3, or radial position parameters from the fits of Equation (1) to each line of dosimeters. Given the estimates of the in-plane (axial) coordinates of the source relative to a given line of dosimeters, the perpendicular distance between the source and the dosimeter plane (e.g. the third spatial coordinate of the source) can be solved by applying the Pythagorean theorem where the length of the hypotenuse of the triangle formed between the source and a given line of detectors is equal to the m_3 parameter given by the fit of Equation (1) to the dose profile. Again, the final estimate of the out-of-plane coordinate was calculated as the variance-weighted average of all of the individual estimates.

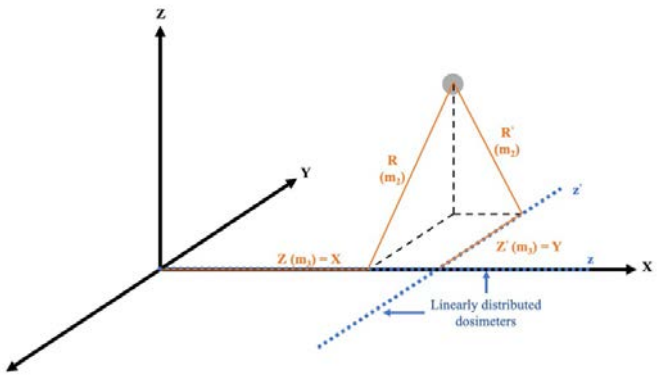

Figure 3: Method for determining the three-dimensional position of a point source using the dose estimates in two orthogonal linear arrays.

With the position estimates determined using the point source approximation, it was hypothesized that an estimate for the source radius would be attainable using forward transport modeling. A simplified model of the exposure geometry was constructing using the MCNP6® code. The modeled geometry included the source, aluminum stand, floor and OSLD arrays. In order to simplify the geometry specification, the utility carts supporting the OSLDs were ignored. Additionally, the OSLD arrays were each modeled as a continuous rectangle of aluminum oxide, AL_2O_3, surrounded by a polyethylene case. Point detector (F5) tallies were placed in the Al_2O_3 region at the locations of the actual dosimeters. While this simplification ignores the spatial extent of the dosimeters, the cost of such a simplification is justified by the greatly reduced computational time required compared to pulse height (*F8) tallies. Further, it is not expected that this approximation will substantially alter the response of the tally compared to the actual energy deposition physics.

2.3 Inverse Transport Methods

The inverse transport problem is a special class of optimization problems where a parameter set in a forward transport model is optimized to match some set of experimental measurements. In many cases, such problems fall into another special class of problems known as black box optimization problems. The term "black box" refers to the non-analytical nature of the forward transport solutions and further, generally implies that gradient information for the parameters of interest is either non-existent or prohibitively expensive to calculate. While many black-box optimization algorithms exist in the literature, this work only focused on relatively simplistic gradient-free, coordinate search methods.

The first, and simplest, solution method (the raster method) consisted of first defining a set of bounds for each of the parameters of interest, the spatial coordinates and radius of the source in this instance, and then computing the chi squared value between simulated and measured doses at equally spaced points within those bounds. Next, the bounds of the previous iteration were moved to bracket the parameter that minimized the chi squared. The subsequent interval was again divided into equally spaced points upon which the chi squared value between simulated and measured doses was calculated. This process of interval refinement was repeated twice and ultimately the parameter value that minimized the chi squared was taken to be the optimal value.

The second method used for the parameter optimization followed the same general approach as the previous method, where each spatial coordinate was optimized independently and sequentially followed by the radius. The main difference was that instead of using a graphical analysis of the chi squared distribution, the second approach used

Brent's method to find the minimum of the chi squared values and the resultant optimum parameter value [7]. The benefit of this approach was that since Brent's method is available in the Scientific Python, *SciPy*, optimization library it was relatively simple to implement and required no interaction with the user [8].

The bounds for each spatial coordinate were selected as a combination of the interval containing the highest dose dosimeters in each direction and any constraints imposed by the physical dimensions of the problem geometry, such as the locations of the floors and the arrays themselves. For example, in the large array, the bounds for the x and y coordinates were taken to be large enough to contain all OSLDs for which a dose greater than 1.6 Gy was measured. This resulted in x-bounds of [-20 cm, 40 cm] and y-bounds of [-25 cm, 45 cm]. The upper boundary of the z-interval was taken to be the largest coordinate of a dosimeter on the small array for which a dose greater than 3 Gy was measured, or between 0 cm and 40 cm, where 0 cm in this case was taken to be the surface aluminum cross plate.

3. Results

Figure 4 shows a graphic rendering of the exposure geometry in addition to the coordinate system used in all of the subsequent analysis and results. The resultant acquired dose profiles for the large and small arrays are shown in Figure 5 and Figure 6 respectively. In these figures, the dose points were plotted on a linear mesh and the resultant dose map surface was generated by linearly interpolating between the measured dose points. Additionally, beneath each surface, in the grid plane, a contour heat map has been plotted.

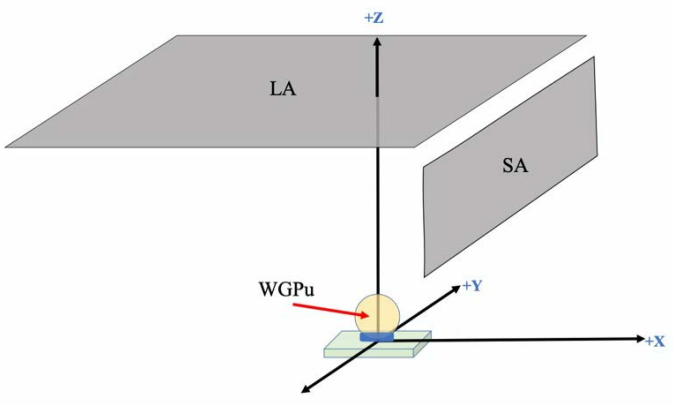

Figure 4: Coordinate system used for the dosimeter arrays with respect to the WGPu source.

The plot in Figure 5 shows an apparent maximum in the dose deposition surface near the (0,0) point in the x-y plane. It was hypothesized that this would be a near optimal measurement scenario since a global maximum implies that the dose measurements have been made on a grid fully containing the source. In contrast, the plot in Figure 6 shows the dose values still increasing at the edge of the z-domain, indicating that the position of the source may fall outside the dose measurement locations in the z-direction. This was indeed the case, as Figure 2 shows, the SA was positioned above the source.

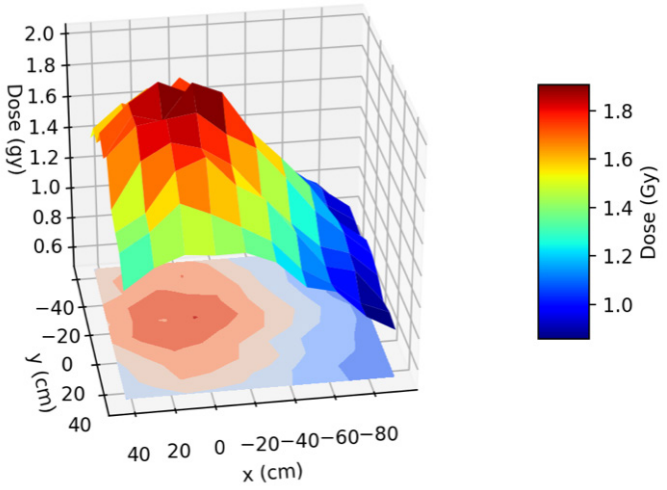

Figure 5: Measured doses to the OSLDs in the large array (LA). The surface map is colored according to the dose, and the doses between adjacent OSLDs were taken as simple linear interpolations. The contour map in the x-y plane shows that a dose gradient exists in both directions, and the OSLD array fully bounded the source distribution.

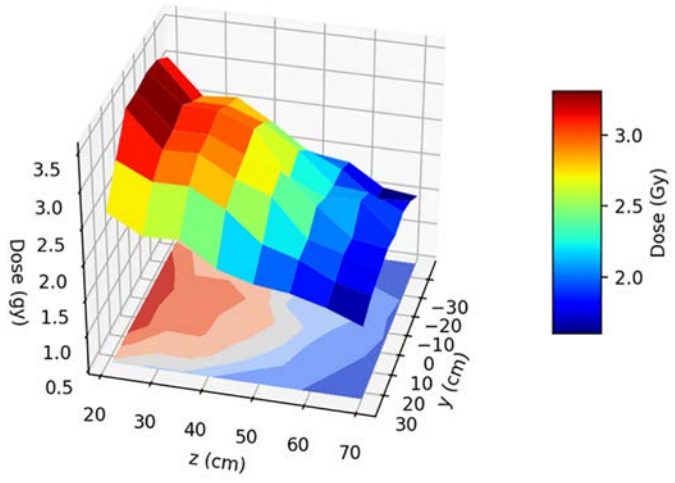

Figure 6: Measured doses to the OSLDs in the small array (SA). The surface map is colored according to the dose, and the doses between adjacent OSLDs were taken as simple linear interpolations. No definite peak is seen in the z-direction, indicating that the dosimeter array does not extend beyond the source location in the z-direction.

Table 1 contains the position estimations calculated from the doses measured in the small and large arrays, respectively, using the analytical method described in Section 2.2. The coordinate system for the dosimeter arrays was defined such that the center of the WGPu sphere was located at position (0,0,4.5) in centimeters.

Array	X (cm)	Y (cm)	Z (cm)
SA	4.4 ± 0.8	-0.2 ± 0.4	10 5
LA	4.6 ± 0.7	-5.6 ± 0.7	2 ± 27

Table 1: Estimated Source Position Coordinates Calculated from the Dosimeters in the Small Array (SA) and Large Array (LA).

It can be seen from the values in Table 1 that the point source approximation method used to estimate the source position tends to poorly resolve all source coordinates. The largest disparity between the assumed true location and the calculated location existed in the y-coordinate estimated from the dosimeters in the large array, followed by the x-coordinate estimates. Referring to the contour plot of the dosimeter measurements in Figure 7, it is apparent that larger measured doses were biased toward the negative y direction. Although steps were taken to align the central axes of each dosimeter array to bisect the center of the source, it is quite reasonable to accept that some uncertainty inevitably existed in the true source locations assumed above. The uncertainty in the x and y positions of the source were taken to be 2 cm each, while the z position uncertainty was taken to be 2 mm. The x and y uncertainty estimates were considerably larger than the z position uncertainty due to the large size of the arrays and the distance between arrays and the source.

It must also be noted that the overall resolution possible in the positional estimates will be inversely correlated to the spacing between the dosimeters, and as result it is expected that observed disagreement between the assumed true and the estimated source positions resulted from a combination of the uncertainty in the true position of the source and resolution limits imposed by the dosimeter spacing chosen. Using the uncertainty estimates for the known source position added in quadrature with position estimate uncertainties, a t-test was performed in order to compare the known source position to the estimates. Table 2 contains the computed *t*-values for each of the coordinates, where the critical *t* at the 95% confidence level was 1.960. It can be seen from the values in Table 2 that only the y-estimate from the SA and the z-estimate from the LA were statistically indistinguishable from the measured values. Therefore, there was disagreement between the known and estimated values that are not accounted for by their associated uncertainties. It was hypothesized that this excess disagreement may have been the result of resolution limits imposed by the spacing of the dosimeters in the arrays.

Array	X	Y	Z
SA	9.13	0.31	3.47
LA	6.87	8.36	0.35

Table 2: t-Statistics Comparing the Known and Estimated Source Positions. Here the null hypothesis was that the known and estimated positions were identical.

Method	Array	X (cm)	Y (cm)	Z (cm)	R(cm)
raster	SA	-1.25	-1.86	10.42	4.49
raster	LA	2.32	-4.86	8.11	4.02
Brent's	SA	5.9	-0.36	18.5	4.22
Brent's	LA	11.0	-9.3	11.1	1.98

Table 3: Estimated Source Position Coordinates Calculated from the Dosimeters in the Small Array (SA) and Large Array (LA).

Table 3 contains the optimum parameters for the source position and radius using each of the inverse transport methodologies described above. It is again apparent that the resolution of the parameter estimates is dependent on the spacing between the dosimeters in the array. One of the challenges with each of the methods tested here was that the total chi-squared values for the arrays were relatively insensitive to changes in the position and source radius for a broad range of values around the true source position. For example, Figure 8 shows the chi-squared value for the simulated and measured dose values for the

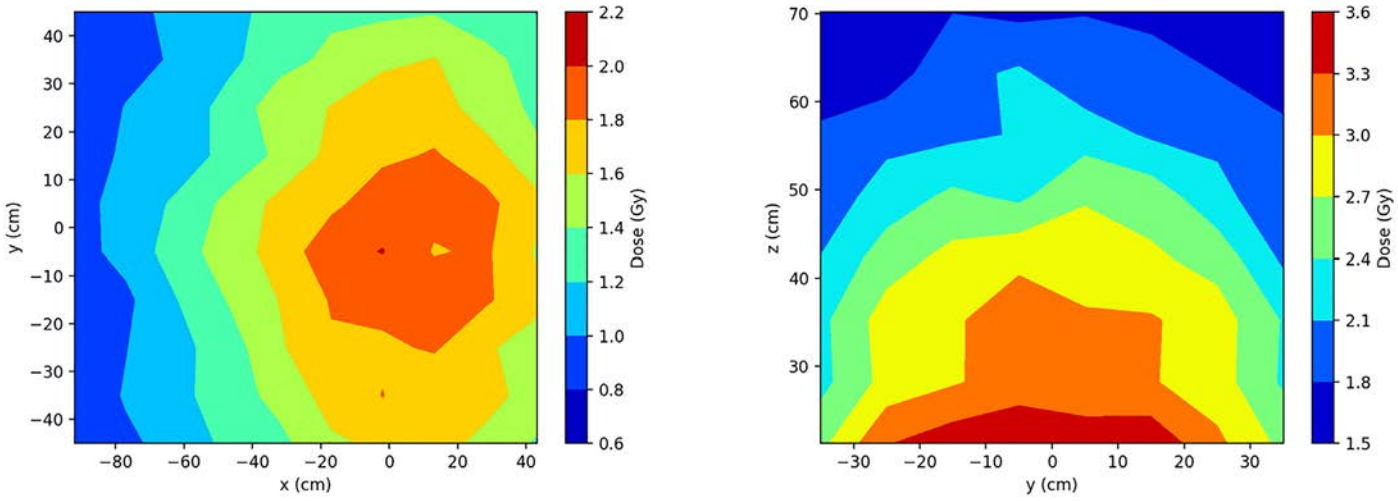

Figure 7: Contour plot of measured doses to the OSLDs in the Large Array (left), and Small Array (right).

dosimeters in the small array. It can be seen that the changes in the computed chi squared were relatively small over a 5-cm range of radius estimates. This problem is compounded by stochastic nosiness inherent to both the measured and simulated element doses resulting in an unavoidable baseline level of noise in the chi squared as a function of position and radius.

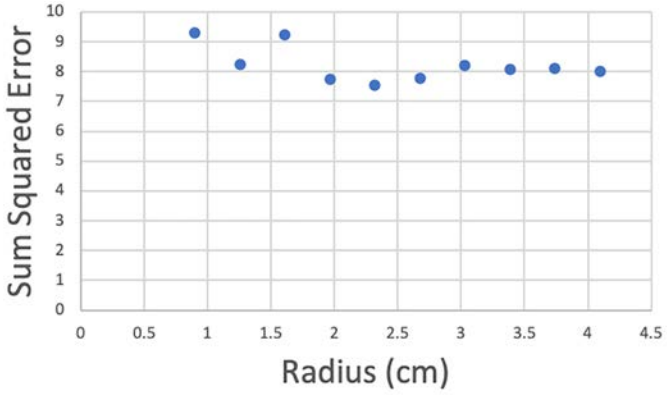

Figure 8: Plot of the chi squared between the simulated and measured dosimeters in the small array as a function of the simulated radius (cm).

Another possible limitation for the raster and Brent's methods is that the final results may be dependent on the order in which the parameters are optimized. The results presented in Table 3 were all computed by optimizing the x-, y-, and z- coordinates followed by the radius. To test this theory, the Brent's method was used to compute estimates for the radius, x-, y-, and z- coordinates (in that order) resulting in estimates that for the radius and x-position (3.73 cm and -5.6 cm, respectively) substantially differed from those presented in Table 3.

4. Conclusions

Previous analyses with a linear array of dosimeters showed promising results for estimating the axial position and radial distance of a source with respect to the line of dosimeters (Hayes and O'Mara, 2020). In this work, two dimensional arrays were used to reconstruct the three-dimensional location of a spherical weapons grade plutonium source. The method consisted of using LM fitting to linearly arrayed dosimeters in orthogonal directions to obtain spatial position estimates. All positional estimates were within 12 cm of the true source position, with the majority of estimates being within 7 cm of the true values. From the position estimates, it was clear that it is important for the dosimeter array to fully contain the profile of the source facing the array. This guarantees that the dose distribution in the array will contain points on each side of the maximum dose.

Using inverse radiation transport methods with coordinate search optimization algorithms, it was again shown that reasonable estimates of the source position (within 10 cm worst case) and source radius (within 2 cm worst case) can be obtained. The major limitation for these methods appeared to be the relatively large range of insensitivity of the chi-squared with respect to the positional and size parameters. Another potential limitation that was discovered during the course of this investigation was that when optimizing multiple parameters, the ordering in which the parameters are optimized can affect the final estimates. The magnitude of this effect, however, can be expected to be inversely proportional to the sensitivity of the results to the parameters being optimized.

In terms of return on investment, the analytical method (Section 1.1) would be the preferable technique for determining the position of a source from a gridded array of dose measurements. Although both of the inverse transport optimization methods required less than 500 model evaluations, and less than 2 hours running time on a single node of a cluster with 32 cores per node, the analytical method returns reasonable results within a matter of seconds on a standard laptop. In terms of making actionable determinations about the presence, or non-presence, of undisclosed source material, the results from the analytical method would be more than sufficient. However, comparable analytical techniques for determining more complex source characteristics such as size, shape, material composition and/or shielding have yet to be developed or tested. As a result, inverse transport optimization methods are, at present, the only and best option for estimating these characteristics. Therefore, future efforts should be devoted to testing the applicability of similar inverse transport optimization methods for estimating more complex, non-positional source characteristics.

Finally, although the dosimetric material used for the dose reconstructions in this study were commercially produced aluminum oxide OSLDs, the ultimate goal is to be able to achieve similar results using minerals derived from ubiquitous materials such as bricks. In general, however, minerals derived from bricks and other earthen based building materials presents additional challenges. Namely, without precise control over the dosimetric material, as there is in commercial OSLDs, there is no guarantee that any samples collected will exhibit sufficient luminescence sensitivity to be useful, especially at low radiation doses. In addition, uncertainties in dose estimates from ubiquitous minerals tend to be higher than those from commercial OSLDs, as a result, the attainable resolution in position and size estimates is decreased for mineral samples. Still, based on the capabilities presented herein, using commercial dosimetry materials, it is likely that the actionable information could be derived using materials derived from environmental materials.

5. Acknowledgements

Acknowledgements to individuals, institutions or funding agencies should be made at the end of the paper before the references.

The authors would like to acknowledge all those who have reviewed these guidelines and contributed to their completion.

6. References

[1] O'Mara, R.P. and Hayes, R.B. *Dose Deposition Profiles in Untreated Brick Material*; *Health Physics*; **114**(4). 2017. 414-420.

[2] Hayes, R.B. and O'Mara, R.P. *Retrospective dosimetry at the natural background level with commercial surface mount resistors; Radiation Measurements*; 112. 2019. 42-48.

[3] Hayes R.B. and O'Mara R.P. *Retrospective Characterization of Special Nuclear Material in Space and Time; Radiation Measurements*; 3. 2020.

[4] Kerns, J.R., Fry, S.F., Sahoo, N., Followill, D.S., Ibbott, G.S. *Angular dependence of the nanoDot OSL dosimeter; Medical Physics;* 38(7). 2011. 3955-3962.

[5] Goorley, T., James, M., Booth, T., Brown, F., Bull, J., Cox, L.J., Durkee, J., Elson, J., Fensin, M., Forster, R.A., Hendricks, J., Hughes, H.G., Johns, R., Kiedrowski, B., Martz, R., Mashnik, S., Mckinney, G., Pelowitz, D., Prael, R., Sweezy, J., Waters, L., Wilcox T., Zukaitis, T. *Initial MCNP6 Release Overview; Nuclear Technology*; 180(**3**). 2010. 298-315.

[6] Bowman S.M. and Gauld I.C. *OrigenARP Primer: How to Perform Isotopic Depletion and Decay Calculations with SCALE/ORIGEN*. ORNL/TM-2010/43, Oak Ridge National Laboratory, Oak Ridge, Tennessee, April 2010.

[7] Brent R.P. *Chapter 4: An Algorithm with Guaranteed Convergence for Finding a Zero of a Function; Algorithms for Minimization without Derivatives*. Prentice-Hall; Englewood Cliffs, NJ. 1973.

[8] Virtanen, P., Gommers, R., Oliphant, T.E., Haberland, M., Reddy, T., Cournapeau, D., Burovski, E., Peterson, P., Weckesser, W., Bright, J., van der Walt, S.J., Brett, M., Wilson, J., Millman, K.J., Mayorov, N., Nelson, A.R.J., Jones, E., Kern, R., Larson, E., Carey, C.J., Polat, I., Feng, Y., Moore, E.W., VanderPlas, J., Laxalde, D., Perktold, J., Cimrman, R., Henriksen, I., Quintero, E.A., Harris, C.R., Archibald, A.M., Ribeiro, A.H., Pedregosa, F., van Mulbregt, P., *SciPy 1.0 Contributors. "SciPy 1.0: Fundamental Algorithms for Scientific Computing in Python; Nature Methods*; 17. 2020. 261-272.